Mechanics of Materials 177 (2023) 104553

Contents lists available at ScienceDirect

Mechanics of Materials

journal homepage: www.elsevier.com/locate/mecmat

Research paper

Stochastic modeling of functionally graded double lap adhesive joints

M.A. Khan [b,d], R. Tipireddy [c], B. Dattaguru [e], S. Kumar [a,f,*]

[a] Materials & Manufacturing Research Group, James Watt School of Engineering, University of Glasgow, Glasgow, G12 8QQ, UK
[b] Department of Mechanical and Materials Engineering, Khalifa University of Science and Technology, PO Box 54224, Abu Dhabi, United Arab Emirates
[c] Pacific Northwest National Laboratory, P.O. Box 999, MSIN K7-90, Richland, WA 99352, USA
[d] Department of Civil Engineering, Mahindra University, Ecole Centrale School of Engineering, Hyderabad, 500043, India
[e] International Institute for Aerospace Engineering and Management, Jain University, Bengaluru, Karnataka, 560069, India
[f] Glasgow Computational Engineering Center, University of Glasgow, Glasgow, G12 8LT, UK

ARTICLE INFO

Keywords:
Double-lap joints
Analytical solutions
Adhesive bonding
Stochastic
Composite materials
Probabilistic mechanics
Polynomial chaos

ABSTRACT

Perturbation(s) in the adhesive's properties originating from the manufacturing, glue-line application method and in-service conditions, may lead to poor performance of bonded systems. Herein, the effect of such uncertainties on the adhesive stresses is analyzed via a probabilistic mechanics framework built on a continuum-based theoretical model. Firstly, a generic 2D plane stress/strain linear-elastic model for a composite double-lap joint with a functionally graded adhesive is proposed. The developed model is validated against the results obtained from an analogous finite element model for the cases of bonded joints with metal/composite adherends subjected to mechanical and thermal loadings. Subsequently, the proposed analytical model is reformulated in probabilistic mechanics framework where the elastic modulus of the adhesive is treated as a spatially varying stochastic field for the cases of homogeneous and graded adhesives. The former case represents stochastic nature of conventional joints with a homogeneous bondline while the later case showcases the perturbation in the properties of functionally graded joints. To propagate the uncertainty in the elastic modulus to shear and peel stresses, we use a non-intrusive polynomial chaos approach. For a standard deviation in the elastic modulus, the proposed model is utilized to evaluate the spatial distribution of shear and peel stresses in the adhesive, together with probability and cumulative distribution functions of their peaks. A systematic parametric study is further carried out to evaluate the effect of varying mean value of the adhesive's Young's moduli, overlap lengths and adhesive thicknesses on the coefficient of variation/standard deviation in peak stresses due to the presence of a random moduli field. It was observed that the joints with stiffer adhesives and longer bondlengths show smaller coefficient of variation in peak stresses. The findings from this study underscore that the predictive capability of the proposed model would be useful for the stochastic design of adhesively bonded joints.

1. Introduction

Adhesively bonded joints enable efficient load-transfer over a larger area and are lighter compared to bolted and welded connections. However, non-uniform distribution of stresses in the adhesive layer is observed. Therefore, peak shear and peel stresses in the bondline have a significant influence on how such connections are designed. Despite having superior load-transfer characteristics compared with their conventional counterparts, they have displayed a wide range of performances. These variations could be attributed to the uncertainties in the geometric and material properties of such systems, arising from manufacturing and in-service conditions (Stroud et al., 2002; Uddin et al., 2004; Luo et al., 2011; Kimiaeifar et al., 2012a; Olajide et al., 2017). Goland and Reissner (1944), first formulated a theoretical model to predict the stresses in flat bonded joints. Since then, a plethora of analytical, numerical and experimental studies investigated the behavior of bonded joints considering different geometric and material properties (Adams and Peppiatt, 1974; Mortensen and Thomsen, 2002; Kumar and Mittal, 2013). Functional gradation of adhesive properties has recently been extensively explored to reduce the peak stresses in the bondline so as to improve the load carrying capacity of the bonded joints (Kumar and Khan, 2016b; Da Silva and Campilho, 2012; Khan et al., 2018b). A simple form of adhesive tailoring combines the favorable characteristics of compliant and brittle adhesives i.e., ductility and strength properties are simultaneously engineered via a graded

* Correspondence to: Professor of Composite Materials and Advanced Manufacturing# 725 Rankine Building, James Watt School of EngineeringOakfield Avenue, University of Glasgow, Glasgow G12 8LT, UK.
E-mail addresses: msv.kumar@glasgow.ac.uk, s.kumar@eng.oxon.org (S. Kumar).

https://doi.org/10.1016/j.mechmat.2022.104553
Received 26 October 2022; Received in revised form 28 December 2022; Accepted 28 December 2022
Available online 4 January 2023

bondline (da Silva and Lopes, 2009; Kumar and Pandey, 2010; Özer and Öz, 2017). Usually, a functionally modulus graded adhesive is implemented in such a way that the bondline has the lowest stiffness near the overlap ends in order to reduce the peak stresses driving failure. For instance, a typical bi-adhesive bondline is engineered to have a single-step change in the modulus of the bondline over the bondlength. On the other hand, a joint with a functionally graded bondline employs a multi-step or smooth variation in adhesive modulus over the bondlength, primarily to optimize the adhesive's stress profile so as to reduce the stress peaks (Stein et al., 2016).

Several studies have reported a decrease in stress concentration in bonded composite joints and patch-repair systems with a functionally graded bondline (Kumar and Scanlan, 2013; Kumar and Khan, 2016b; Khan and Kumar, 2016). The experimental evidence showcasing performance enhancements in terms of strength by the application of functionally graded bondline can be noted from some of the studies in which adhesive tailoring was realized by selective placement of glass beads or nano-silica inclusions (Stapleton et al., 2012), graded curing via induction heating (Carbas et al., 2014) and functional dispersion of carbon black with dielectric heating (Carbas et al., 2017). In order to demonstrate functional gradation of bondlayer's properties of a single-lap joint, advanced manufacturing techniques, including 3D printing were employed (Kumar et al., 2016). This resulted in a greater than 100% increase in the joints' toughness and load carrying capacity. This work was extended to explore the effect of bondlayer and adherend tailoring of bonded systems with varying geometries (Khan and Kumar, 2018; Khan et al., 2018a; Ubaid et al., 2018) and similar observations on strength and toughness enhancements were noted.

Some of the uncertainties associated with the adhesive phase are due to poor mixing, laying pattern/filling that could lead to a cluster of micro-voids due to entrapment of air, volatiles and chemical reactions, defined as porosity in adhesives (Katnam et al., 2011). The porosity exists in most of the bondlines to a certain degree (Adams, 2018). Partial cure can occur due to not following the cure profile, incorrect mixing of the adhesive, wrong formulation, or insufficient thermal exposure (Katnam et al., 2011). Partial curing, stresses and thermal shrinkage could lead to adhesive cracking (Omairey et al., 2021). As a consequence, adhesively bonded joints show a significant variation in performance and therefore, a few studies have focused on quantifying such uncertainties. Yu et al. (2019) studied the variations in the ratio of bond strength to model predictions and concluded that these variations are highly dependent on input parameters rather than being completely random. They obtained bond strength values from an experimental database gathered from literature while they used the classical solution of Hart-Smith (1973) as a predictive model. A similar observation was made by Zhang et al. (2018) while examining the model uncertainties against the experimental results. Kimiaeifar et al. (2012b) developed a probabilistic model based on 3D Finite Element Method (FEM) for adhesively bonded scarf joints which helped to calibrate partial safety factors with respect to variations in input data. They extended the model to assess the reliability of such joints (Kimiaeifar et al., 2013). Bhat et al. (2015) carried out FE analysis on single-lap joints by considering geometric and material parameters as stochastic variables with a log-normal distribution. They demonstrated how variations in the adherend thickness and the adhesive stiffness affect the peak stresses in the adhesive layer. Mathias and Lemaire (2013) assessed the variability in adhesive shear and peel stresses by treating the thickness of the adhesive as a spatially varying stochastic field, employing a probabilistic mechanics based FE framework. Functional tailoring of adhesive's properties is a niche technology that has known manufacturing challenges. However, to the best of authors' knowledge, there have only been a few studies that attempted to quantify the effect of such uncertainties. For instance, in their analyses of bonded anchors with a degraded bondline, Tipireddy and Kumar (2017) regarded the shear stiffness of the adhesive as a stochastic field.

The proposed study focuses on modeling aspects of functionally graded adhesive joints and has two parts. The first component of it presents a deterministic continuum-based model for predicting adhesive stresses in an adhesively bonded double-lap joint (DLJ) with a functionally graded bondline. In the second part of the study, the elastic modulus of the adhesive is regarded as a spatially varying stochastic field with a homogeneous or graded mean, formulating the problem in the probabilistic mechanics framework via a non-intrusive polynomial chaos approach. This allows us to investigate the deviations in the adhesive stresses with the help of probability and cumulative distribution functions of stress peaks. For the case study where the stochastic field has a homogeneous mean, we focus on the variation in adhesive stresses that stems from manufacturing defects in conventional joints with ungraded/non-tailored adhesive. In the later case, we quantify the effect of uncertainties in the adhesive properties of a functionally graded DLJ on the bondline stresses. A systematic parametric study is carried out to quantify the deterministic variations and uncertainties in adhesive stresses for a practical range of geometric and material parameters, in the presence of a stochastic bondline. Furthermore, we quantify such uncertainties in terms of standard deviation and coefficient of variation in peak shear and peel stresses.

2. Deterministic model for adhesive stresses

Fig. 1a depicts an idealization of an adhesively bonded DLJ under an axial tensile load P. The overlap region of the assembly with length l and layer thickness h_i is shown in Fig. 1b. The top and the middle adherends experience axial tensile stresses of magnitude σ_0 and $\rho\sigma_0$, respectively. All the traction and traction-free conditions at the respective boundaries are indicated in Fig. 1c. Here, the subscript $i = 1, 2$ and a refers to the top adherend, middle adherend and the adhesive, respectively. Note that, at the plane of symmetry, the distortion is zero. Therefore, the shear stress in the middle adherend at this plane vanishes i.e., $\sigma^{(2)}_{xy}(x, 0) = 0$. However, the normal component of the traction exists i.e., $\sigma^{(2)}_{yy}(x, 0) \neq 0$. In DLJs, although the adherends are subjected to axial loads, the eccentric load-path leads to high transverse deformation, resulting in bending stresses. Theoretical formulations to incorporate the bending stresses in bonded joints were developed by several groups, see for example (Stein et al., 2016; Khan et al., 2018b; Kumar and Khan, 2016b). One of the simplifying assumptions we make here is to neglect the effect of bending due to the balanced nature of DLJs. Therefore, the axial stresses in each of the members is independent of the transverse coordinate y, i.e., $\sigma^{(1)}_{xx} = \sigma^{(1)}_{xx}(x)$, $\sigma^{(2)}_{xx} = \sigma^{(2)}_{xx}(x)$ and $\sigma^{(a)}_{xx} = \sigma^{(a)}_{xx}(x) = \sigma_a$. Henceforth, for brevity, the axial stresses in the top adherend, middle adherend and the adhesive are denoted by σ_1, σ_2 and σ_a, respectively. From elasto-statics, neglecting body forces, the governing differential equations of equilibrium for generalized plane strain/stress problem, is given by

$$\frac{\partial \sigma^{(i)}_{xx}}{\partial x} + \frac{\partial \sigma^{(i)}_{xy}}{\partial y} = 0 \tag{1}$$

$$\frac{\partial \sigma^{(i)}_{xy}}{\partial x} + \frac{\partial \sigma^{(i)}_{yy}}{\partial y} = 0 \tag{2}$$

Since, the axial/longitudinal stress in any member is independent of $y-$coordinate, the shear and peel stresses in member $'i'$ can be expressed as:

$$\sigma^{(i)}_{xy} = \int_y \frac{d}{dx}\left(\sigma_i\right)\, dy = f^{(i)}_1(x) + y\,\sigma'_i \tag{3}$$

$$\sigma^{(i)}_{yy} = \int_y \frac{d}{dx}\left(\sigma^{(i)}_{xy}\right)\, dy = f^{(i)}_2(x) + \frac{d}{dx}\left(f^{(i)}_1(x)\right)\, y + \frac{y^2}{2}\sigma''_i \tag{4}$$

where, $f^{(i)}_1(x)$ and $f^{(i)}_2(x)$ are unknown functions needed to satisfy the equilibrium equations and σ' denotes derivative of the function $\sigma(x)$ with respect to axial coordinate$-x$. The exact forms of $f^{(i)}_1(x)$ and $f^{(i)}_2(x)$

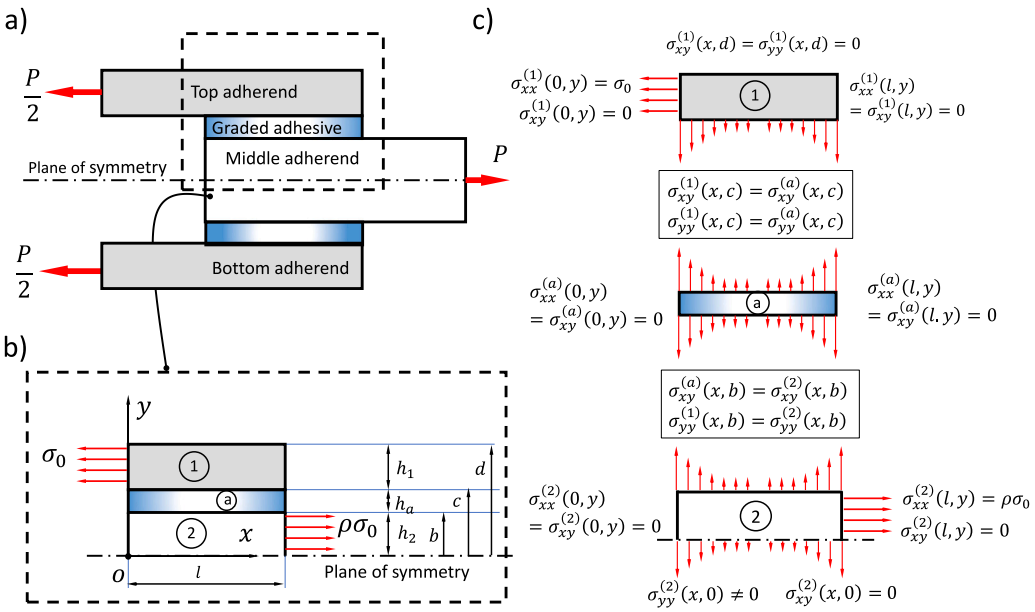

Fig. 1. (a) Idealization of a DLJ subjected to an axial tensile load P. (b) A sandwich multi-layer model, taken directly from the DLJ. (c) Free-body diagram of the sandwich model with traction boundary conditions. Note that the adhesive is treated as an isotropic bondline, while the adherends are regarded as homogeneous orthotropic composites.

are obtained by satisfying the traction-free and traction-continuity conditions at the lateral surfaces. From Eqs. (3) and (4), we note that the shear and peel stresses in each of the members are functions of axial stresses and their derivatives. The global axial force equilibrium of the assembly shown in Fig. 1b yields the following relationship between the axial stresses σ_1, σ_2 and σ_a:

$$\sigma_1\rho + \sigma_a r + \sigma_2 = \rho\sigma_0 \tag{5}$$

where,

$$\rho = \frac{h_1}{h_2} \quad ; \quad r = \frac{h_a}{h_2} \tag{6}$$

Using the above equation, we write the axial stress in the middle adherend σ_2 in terms of axial stresses in the top adherend σ_1 and the adhesive σ_a, leading to a reduction in number of fundamental unknowns to two i.e., σ_1 and σ_a. The shear and peel stresses in the top adherend are obtained by satisfying traction-free conditions at $y = d$ i.e., by substituting $\sigma^{(1)}_{xy}(x,d) = \sigma^{(1)}_{yy}(x,d) = 0$ into Eqs. (3) and (4):

$$\sigma^{(1)}_{xy} = (d-y)\frac{d\sigma_1}{dx} \tag{7}$$

$$\sigma^{(1)}_{yy} = (d-y)^2\frac{d^2\sigma_1}{dx^2} \tag{8}$$

The shear and peel stresses in the adhesive bondlayer are derived by satisfying the traction continuity at the interface $y = c$ between the top adherend and the adhesive. Note that the continuity conditions of stresses at $y = c$, are $\sigma^{(1)}_{xy}(x,c) = \sigma^{(a)}_{xy}(x,c)$ and $\sigma^{(1)}_{yy}(x,c) = \sigma^{(a)}_{yy}(x,c)$. Substitution of these conditions in Eqs. (3), (4), (7) and (8), yields the following expressions for the shear and peel stresses in the adhesive:

$$\sigma^{(a)}_{xy} = (c-y)\frac{d\sigma_a}{dx} + h_1\frac{d\sigma_1}{dx} \tag{9}$$

$$\sigma^{(a)}_{yy} = \frac{1}{2}\left((c-y)^2\frac{d^2\sigma_a}{dx^2} + \left[h_1^2 + 2h_1(c-y)\right]\frac{d^2\sigma_1}{dx^2}\right) \tag{10}$$

The axial/longitudinal stress in the middle adherend in terms of primary unknowns is obtained from Eq. (5) and is written as:

$$\sigma_2 = \rho\,(\sigma_0 - \sigma_1) - r\,\sigma_a \tag{11}$$

Akin to the previous step, the shear and peel stresses in the middle adherend are derived using the continuity conditions of stresses at the interface $y = b$, by imposing $\sigma^{(a)}_{xy}(x,b) = \sigma^{(2)}_{xy}(x,b)$ and $\sigma^{(a)}_{yy}(x,b) = \sigma^{(2)}_{yy}(x,b)$. Substituting these conditions in Eqs. (3) and (4) while satisfying Eqs. (9) and (10) at the interface $y = b$, we obtain expressions for the shear and peel stresses in the middle adherend as:

$$\sigma^{(2)}_{xy} = y\left[\rho\frac{d\sigma_1}{dx} + r\frac{d\sigma_a}{dx}\right] \tag{12}$$

$$\sigma^{(2)}_{yy} = \frac{y}{2}\left[\left((k + h_2^2\rho) - y^2\rho\right)\frac{d^2\sigma_1}{dx^2} + \left((h_a^2 + rh_2^2) - y^2 r\right)\frac{d^2\sigma_a}{dx^2}\right] \tag{13}$$

where,

$$k = h_1^2 - 2h_1h_2 + 2ch_1; \qquad c = h + h_a; \tag{14}$$

Note that the stresses in each of the members are in terms of the primary unknown stress functions σ_1 and σ_a. Therefore, the elastic strains in each member i could be expressed in terms of σ_1 and σ_a employing a generalized plane-stress/strain linear thermo-elastic orthotropic constitutive relations expressed as:

$$\varepsilon^{(i)}_{xx} = S^{(i)}_{11}\sigma^{(i)}_{xx} + S^{(i)}_{12}\sigma^{(i)}_{yy} + \varepsilon^{(i)}_{tx} \tag{15}$$

$$\varepsilon^{(i)}_{yy} = S^{(i)}_{12}\sigma^{(i)}_{xx} + S^{(i)}_{22}\sigma^{(i)}_{yy} + \varepsilon^{(i)}_{ty} \tag{16}$$

$$\varepsilon^{(i)}_{xy} = S^{(i)}_{66}\sigma^{(i)}_{xy} \tag{17}$$

where, $\varepsilon^{(i)}_{tx}$ and $\varepsilon^{(i)}_{ty}$ are thermal strains in the x and y directions, respectively. The components of the compliance matrix $S^{(i)}_{mn}$ are presented in Table 1 for the plane-strain/stress formulations. Note that these components are dependent on the spatial coordinates for the functionally graded bondline. Using the stresses and the strains expressed before, the complementary strain energy density for each of the member $'i'$ can be expressed as:

$$U^{(i)}_d = \frac{1}{2}\sigma^{(i)}_{mn}\epsilon^{(i)}_{mn} = \frac{1}{2}\left[S^{(i)}_{11}\left(\sigma^{(i)}_{xx}\right)^2 + S^{(i)}_{22}\left(\sigma^{(i)}_{yy}\right)^2 + 2S^{(i)}_{12}\sigma^{i}_{xx}\sigma^{(i)}_{yy} + 2S^{(i)}_{66}\left(\sigma^{(i)}_{xy}\right)^2 + \sigma^{(i)}_{xx}\epsilon^{(i)}_{tx} + \sigma^{(i)}_{yy}\epsilon^{(i)}_{ty}\right] \tag{18}$$

Integrating the complementary energy density over the volume, the total complementary energy is obtained as:

$$U = \sum_i \int_l\int_y U^{(i)}_d\,dx\,dy = \int_l\int_0^b U^{(1)}_d\,dx\,dy + \int_l\int_c^d U^{(2)}_d\,dx\,dy + \int_l\int_b^c U^{(a)}_d\,dx\,dy \tag{19}$$

Table 1
Constitutive relation for the members based on plane-stress/plane-strain formulation with Orthotropic/Isotropic materials. Note that the adherends can be Orthotropic/Isotropic but the adhesive is always Isotropic with/without gradation.

Case	$S_{11}^{(i)}$	$S_{22}^{(i)}$	$S_{12}^{(i)}$	$S_{66}^{(i)}$	$\epsilon_{tx}^{(i)}$	$\epsilon_{ty}^{(i)}$
Plane-strain Orthotropic	$\frac{1}{E_x^{(i)}}\left(1-\nu_{zx}^{(i)}\nu_{xz}^{(i)}\right)$	$\frac{1}{E_y^{(i)}}\left(1-\nu_{zy}^{(i)}\nu_{yz}^{(i)}\right)$	$\frac{1}{E_x^{(i)}}\left(\nu_{xy}^{(i)}-\nu_{zy}^{(i)}\nu_{xz}^{(i)}\right)$	$\frac{1}{2G_{xy}^{(i)}}$	$\left(\nu_{zx}^{(i)}\alpha_z^{(i)}+\alpha_x^{(i)}\right)\Delta T^{(i)}$	$\left(\nu_{zy}^{(i)}\alpha_z^{(i)}+\alpha_y^{(i)}\right)\Delta T^{(i)}$
Plane-stress Orthotropic	$\frac{1}{E_x^{(i)}}$	$\frac{1}{E_y^{(i)}}$	$-\frac{\nu_{xy}^{(i)}}{E_x^{(i)}}$	$\frac{1}{2G_{xy}^{(i)}}$	$\alpha_x^{(i)}\Delta T^{(i)}$	$\alpha_y^{(i)}\Delta T^{(i)}$
Plane-strain Isotropic	$\frac{1-(\nu^{(i)})^2}{E^{(i)}}$	$\frac{1-(\nu^{(i)})^2}{E^{(i)}}$	$-\frac{\nu^{(i)}+(\nu^{(i)})^2}{E^{(i)}}$	$\frac{1}{2G^{(i)}}$	$(1+\nu^{(i)})\alpha^{(i)}\Delta T^{(i)}$	$(1+\nu^{(i)})\alpha^{(i)}\Delta T^{(i)}$
Plane-stress Isotropic	$\frac{1}{E^{(i)}}$	$\frac{1}{E^{(i)}}$	$-\frac{\nu^{(i)}}{E^{(i)}}$	$\frac{1}{2G^{(i)}}$	$\alpha^{(i)}\Delta T^{(i)}$	$\alpha^{(i)}\Delta T^{(i)}$

Substitution of stresses given by Eqs. (7) to (13) into the total complementary strain energy, yields

$$U = \phi_1\,\sigma_1^2+\phi_2\,\sigma_a^2+\phi_3\left(\sigma_1'\right)^2+\phi_4\left(\sigma_a'\right)^2+\phi_5\left(\sigma_1''\right)^2+\phi_6\left(\sigma_a''\right)^2 + \phi_7\,\sigma_1'\sigma_a'+\phi_8\,\sigma_1\sigma_1''+\phi_9\,\sigma_a\sigma_a''+\phi_{10}\,\sigma_1''\sigma_a''+\phi_{11}\,\sigma_1 + \phi_{12}\,\sigma_a+\phi_{13}\,\sigma_1''+\phi_{14}\,\sigma_a''+\phi_{15} \tag{20}$$

where, $\phi_1,\phi_2,\ldots,\phi_{15}$ are obtained by substitution of stress fields in Eq. (15) and (18). Minimization of the complementary strain energy functional in conjunction with calculus of variation renders the following coupled ordinary differential equations (ODEs):

$$A_{\alpha\beta}\begin{pmatrix}\frac{d^4\sigma_1}{dx^4}\\ \frac{d^4\sigma_a}{dx^4}\end{pmatrix}+B_{\alpha\beta}\begin{pmatrix}\frac{d^3\sigma_1}{dx^3}\\ \frac{d^3\sigma_a}{dx^3}\end{pmatrix}+C_{\alpha\beta}\begin{pmatrix}\frac{d^2\sigma_1}{dx^2}\\ \frac{d^2\sigma_a}{dx^2}\end{pmatrix}+D_{\alpha\beta}\begin{pmatrix}\frac{d\sigma_1}{dx}\\ \frac{d\sigma_a}{dx}\end{pmatrix}+F_{\alpha\beta}\begin{pmatrix}\sigma_1\\ \sigma_a\end{pmatrix} = -J_\alpha \tag{21}$$

where, α and β range over 1–2, $A_{\alpha\beta}$, $B_{\alpha\beta}$, $C_{\alpha\beta}$, $D_{\alpha\beta}$, $F_{\alpha\beta}$ and J_α depend on the configuration of the DLJ and loading, and are given in Appendix.

The traction and traction-free conditions at the left and the right boundaries are utilized to obtain the boundary conditions in order to solve the above governing ODEs. These conditions are prescribed as

$$\sigma_1(0)=\sigma_0;\ \sigma_1(l)=0;\ \sigma_1'(0)=0;\ \sigma_1'(l)=0 \tag{22}$$

$$\sigma_a(0)=0;\ \sigma_a(l)=0;\ \sigma_a'(0)=0;\ \sigma_a'(l)=0 \tag{23}$$

The solution of two governing ODEs along with the boundary conditions given above gives the fundamental unknowns σ_1 and σ_a. These axial stresses are then used to predict the shear and peel stresses in the DLJs with deterministic moduli profiles.

3. Stochastic framework for adhesive stresses

The deterministic analytical model for an adhesively bonded DLJ described in the previous section is modified in a stochastic framework to account for the uncertainty in the material properties and obtain a stochastic model. Elastic modulus of the adhesive layer has a significant effect on the performance of a bonded assembly (Kim et al., 1989) as it influences the distribution of adhesive stresses (Khan et al., 2018a,b). Therefore, the elastic modulus of the adhesive is modeled as a spatially varying random field. Let $E^{(a)}(x,\omega)$ be the elastic modulus of the bondline, modeled to vary spatially over x-coordinate and $\omega\in\Omega$ is an outcome of a random experiment, where $(\Omega,\mathcal{F},\mathcal{P})$ is a complete probability space with sample space, Ω, σ-algebra $\mathcal{F}$ and probability measure $\mathcal{P}$ (Ghanem and Spanos, 1991; Lévy and Loève, 1965; Babuška and Chatzipantelidis, 2002). Random elastic modulus induces uncertainty in the stress components $(\sigma_{pq}^{(i)}(x,y,\omega))$, the strain components $(\epsilon_{pq}^{(i)}(x,y,\omega))$. Here, the compliance matrix $(S_{mn}(x,\omega))$ = a function of random elastic modulus, is independent of transverse direction, as we are grading only along bondlength. Also, note that the primary unknowns in this case are the spatially varying stochastic fields $\sigma_1(x,\omega)$ and $\sigma_a(x,\omega)$. Repeating the procedure employed in the previous section i.e., constructing strain–energy functional and minimizing it with respect to the primary unknowns using Euler–Lagrange variational principle, following set of coupled governing stochastic differential equations (SDEs) are obtained:

$$A_{\alpha\beta}\begin{pmatrix}\frac{d^4\sigma_1(x,\omega)}{dx^4}\\ \frac{d^4\sigma_a(x,\omega)}{dx^4}\end{pmatrix}+B_{\alpha\beta}\begin{pmatrix}\frac{d^3\sigma_1(x,\omega)}{dx^3}\\ \frac{d^3\sigma_a(x,\omega)}{dx^3}\end{pmatrix}+C_{\alpha\beta}\begin{pmatrix}\frac{d^2\sigma_1(x,\omega)}{dx^2}\\ \frac{d^2\sigma_a(x,\omega)}{dx^2}\end{pmatrix}+D_{\alpha\beta}\begin{pmatrix}\frac{d\sigma_1(x,\omega)}{dx}\\ \frac{d\sigma_a(x,\omega)}{dx}\end{pmatrix} + F_{\alpha\beta}\begin{pmatrix}\sigma_1(x,\omega)\\ \sigma_a(x,\omega)\end{pmatrix} = -J_\alpha. \tag{24}$$

Here, the elastic modulus of the adhesive layer is modeled as a random field with log-normal distribution, i.e., $E(x,\omega)=\exp[H(x,\omega)]$, where, $H(x,\omega)$ is Gaussian random field with mean $H_m(x)$ and following CoVariance function,

$$C_H(x_1,x_2)=\sigma_H^2\exp\left(-\frac{|x_1-x_2|}{l_x^2}\right), \tag{25}$$

where, σ_H is the standard deviation and l_x is the correlation length of the random field $H(x,\omega)$.

For numerical implementation, Gaussian random field, $H(x,\omega)$ is approximated using a truncated Karhunen–Loève (KL) (Lévy and Loève, 1965; Ghanem and Spanos, 1991; Tipireddy and Ghanem, 2014) expansion to convert infinite dimensional random field into a finite dimensional one, as follows,

$$H(x,\omega)\approx H(x,\boldsymbol{\xi})=H_m(x)+\sum_{i=1}^{d}H_i(z)\sqrt{\lambda_i}\,\boldsymbol{\xi_{i(\omega)}} \tag{26}$$

where, $\boldsymbol{\xi}=(\xi_1,\ldots,\xi_d)^T$, and $\xi_i\sim N(0,1)$ are uncorrelated standard Gaussian random variables and hence are also independent. H_m is the mean of the random field $H(x,\omega)$, and $\{H_i(x)\}$ and $\{\lambda_i\}$ are eigenfunctions and eigenvalues of $C_H(x_1,x_2)$ obtained by solving the following integral eigenvalue problem:

$$\int_0^l C_H(x_1,x_2)\,H_i(x_2)\,dx_2=\lambda_i H_i(x_1). \tag{27}$$

The eigenvalues $\{\lambda_i\}$ are positive and non-increasing (see Tipireddy and Kumar, 2017) and hence the KL expansion in (26) can be truncated after $d+1$ terms, and the eigenfunctions $\{H_i(x)\}$ are orthonormal, i.e.,

$$\int_0^l H_i(x)\,H_j(x)\,dz=\delta_{ij}, \tag{28}$$

where, δ_{ij} is the Kronecker delta. Now, the elastic modulus of the bondline $E(x,\omega)$ can be approximated with a truncated polynomial chaos expansion as follows,

$$E^{(a)}(x,\omega)\approx E^{(a)}(x,\boldsymbol{\xi})=E_m(x)+\sum_{i=1}^{p}E_i(x)\,\psi_i(\boldsymbol{\xi}), \tag{29}$$

where, E_m is the mean, E_i are polynomial chaos coefficients and $\psi_i(\boldsymbol{\xi})$ are multi-variate Hermite polynomials in $\boldsymbol{\xi}=\left[\xi_1,\ldots,\xi_d\right]^T$, that are orthonormal with respect to the probability density of $\boldsymbol{\xi}$, i.e.,

$$\int_\Omega \psi_i(\boldsymbol{\xi})\,\psi_j(\boldsymbol{\xi})\,d\boldsymbol{\xi}=\delta_{ij}. \tag{30}$$

Here, $p+1=\frac{(M+d)!}{M!d!}$ is the number of terms in the expansion, where M is the degree of polynomial chaos expansion and d is the dimension.

The fundamental unknown axial stresses $\sigma_1(x,\omega)$ and $\sigma_a(x,\omega)$, can be expanded using a truncated polynomial chaos as follows:

$$\sigma_1(x,\omega) \approx \sigma_1(x,\xi) = \sigma_{1m}(x) + \sum_{i=1}^{p} \sigma_{1i}(x)\psi_i(\xi), \tag{31}$$

$$\sigma_a(x,\omega) \approx \sigma_a(x,\xi) = \sigma_{am}(x) + \sum_{i=1}^{p} \sigma_{ai}(x)\psi_i(\xi), \tag{32}$$

where, σ_{1m}, σ_{am} are the mean values, σ_{1i} and σ_{ai} are the polynomial chaos coefficients of the stresses $\sigma_1(x,\omega)$ and $\sigma_a(x,\omega)$, respectively. Coupled SDE (24) can be rewritten in terms of ξ as:

$$A_{\alpha\beta}\begin{pmatrix}\frac{d^4\sigma_1(x,\xi)}{dx^4}\\ \frac{d^4\sigma_a(x,\xi)}{dx^4}\end{pmatrix} + B_{\alpha\beta}\begin{pmatrix}\frac{d^3\sigma_1(x,\xi)}{dx^3}\\ \frac{d^3\sigma_a(x,\xi)}{dx^3}\end{pmatrix} + C_{\alpha\beta}\begin{pmatrix}\frac{d^2\sigma_1(x,\xi)}{dx^2}\\ \frac{d^2\sigma_a(x,\xi)}{dx^2}\end{pmatrix}$$
$$+D_{\alpha\beta}\begin{pmatrix}\frac{d\sigma_1(x,\xi)}{dx}\\ \frac{d\sigma_a(x,\xi)}{dx}\end{pmatrix} + F_{\alpha\beta}\begin{pmatrix}\sigma_1(x,\xi)\\ \sigma_a(x,\xi)\end{pmatrix} = -J_\alpha. \tag{33}$$

In order to solve the above governing SDEs, a non-intrusive stochastic collocation approach (Xiu and Karniadakis, 2002; Babuška et al., 2007) is adopted, in which, Eq. (33) are solved at a few realizations of the random variables called quadrature points with respect to their probability measure. Let $\xi^{(q)}$ be the quadrature points of the underlying random variables, ξ, then following deterministic equations are solved,

$$A_{\alpha\beta}\begin{pmatrix}\frac{d^4\sigma_1(x,\xi^{(q)})}{dx^4}\\ \frac{d^4\sigma_a(x,\xi^{(q)})}{dx^4}\end{pmatrix} + B_{\alpha\beta}\begin{pmatrix}\frac{d^3\sigma_1(x,\xi^{(q)})}{dx^3}\\ \frac{d^3\sigma_a(x,\xi^{(q)})}{dx^3}\end{pmatrix} + C_{\alpha\beta}\begin{pmatrix}\frac{d^2\sigma_1(x,\xi^{(q)})}{dx^2}\\ \frac{d^2\sigma_a(x,\xi^{(q)})}{dx^2}\end{pmatrix}$$
$$+D_{\alpha\beta}\begin{pmatrix}\frac{d\sigma_1(x,\xi^{(q)})}{dx}\\ \frac{d\sigma_a(x,\xi^{(q)})}{dx}\end{pmatrix} + F_{\alpha\beta}\begin{pmatrix}\sigma_1(x,\xi^{(q)})\\ \sigma_a(x,\xi^{(q)})\end{pmatrix} = -J_\alpha. \tag{34}$$

for $q = 1,\ldots,n_q$, where n_q is the total number of quadrature points required. Polynomial chaos coefficients $w_i(z)$ of the random field $w(z,\xi)$ are obtained by projecting $w(z,\xi)$ on to the polynomial $\psi_i(\xi)$ as

$$\begin{aligned} w_i(z) &= \mathbb{E}\left[w(z,\xi)\psi_i(\xi)\right] \\ &= \int_\Omega w(z,\xi)\psi_i(\xi)d\xi \\ &\approx \sum_{q=1}^{n_q} w(z,\xi^{(q)})\psi_i(\xi^{(q)})\mu^{(q)}, \end{aligned} \tag{35}$$

where, $\xi^{(q)} = [\xi_1^{(q)},\ldots,\xi_d^{(q)}]^T$ is the quadrature point and $\mu^{(q)}$ is the corresponding weight.

4. Finite element (FE) validation for adhesive stresses in DLJs with deterministic modulus profile

4.1. Finite element modeling

Finite element analyses (FEA) were performed on double-lap bonded assemblies with geometric and material properties similar to those of the analytical model, using Abaqus FEA version 6.14. Utilizing the symmetry of a DLJ, one-half portion was modeled by placing rollers (applying lateral restraint) along the length at the mid-height of the middle adherend as depicted in Fig. 2. A tensile stress, representing an axial force, was applied on the top adherend at the left-end, while a longitudinal restraint was provided at the right-end of the middle adherend. The geometry was modeled as a sandwich with small overhangs and is symmetric with respect to x-axis. Note that the geometry, loading and boundary conditions are similar to those of analytical model (see Fig. 1). A refined mesh containing four noded bilinear plane-strain quadrilateral elements (CPE4R) of size 0.025 mm × 0.025 mm were used for both the adherends and the adhesive. An initial temperature of 0 °C was applied uniformly over the entire geometry. For thermal analysis, during the loading step, the temperature field of the assembly was changed uniformly to −113 °C, in order to evaluate the thermal stresses induced in the system. The adherends were allowed to be orthotropic-/isotropic-continuum while the bondline was treated as a functionally graded isotropic-continuum. Although the adhesive was treated as a functionally graded material, the Poisson's ratio was kept constant over the bondlength akin to Kumar (2009). User defined subroutine called UMAT (written in FORTRAN) was developed to implement material models for graded bondlines.

The predictions from the proposed analytical model with plane-strain constitutive model were validated against the results obtained from analogous FE models for the configurations of the DLJ given in Table 2. From Table 2, note the lowest value of the elastic modulus of graded bondline, $E_0 = 0.28$ GPa and the highest value, $E_m = 3.92$ GPa. The minimum and maximum values of modulus were chosen considering a range of epoxy adhesives available commercially. Such a large variation in the bondline stiffness is examined here to see its effect on the stress-state. Also, we extended such analysis to analyze deviations in adhesive stresses in the functionally modulus graded bondline.

4.2. Metal-to-metal joints under mechanical loading

In the first numerical example, theoretical and FE analyses were carried out on a DLJ comprising titanium adherends and a non-tailored bondline (Epoxy adhesive) with geometric properties $l = 50$ mm, $h_1 = h_2 = 2$ mm, and $h_a = 0.2$ mm. These properties were used as baseline joint configuration of the DLJ unless specified otherwise. Fig. 3 shows the shear and peel stresses along the overlap length at the mid-surface of the adhesive, obtained both from analytical model and FEA. It can be seen that the stresses predicted by the proposed deterministic model and the FEA are in good agreement with each other. Note that a discrepancy is observed in the peel stress predicted by the analytical model closer to the left-end of the joint in comparison to FE results which could be attributed to the simplifying assumption of neglecting bending stresses. However, the peak values of peel stresses obtained from the model match well with those obtained from FEA. Note that for the baseline case with non-tailored epoxy adhesive with titanium adherends, the bondlength ($l = 50$ mm) can be regarded as a critical shear-transfer-length l_{cr}. l_{cr} is the minimum length beyond which the shear and peel stress peaks saturate (as a function of overlap length) and can be defined as the minimum length required to enable a complete load transfer in shear. It could be identified by a region of zero shear stress in the mid-overlap region of the bondline (Kumar and Khan, 2016a).

From Fig. 3, it can be observed that the peak shear and peel stresses occur at the free edges. These observations are frequently reported in the stress analysis of bonded joints (see for instance Khan et al., 2018b; Kumar, 2009; Khan et al., 2022). As discussed in the preceding sections, adhesive tailoring is employed to reduce these stress concentrations. A two-sided parabolic gradation of the modulus profile of the bondline with a maximum value (E_m) at the mid-bondlength and a minimum value (E_0) at the ends of the overlap is adopted here such that:

$$E^{(a)}(x) = 4(E_m - E_0)\left(\frac{x}{l}\right)\left(1 - \left(\frac{x}{l}\right)\right) + E_0 \tag{36}$$

Fig. 3 shows the comparison of shear and peel stresses along the overlap length obtained for the joint with non-tailored adhesive with those of the graded/tailored one both from the analytical model and FE simulation. For the parameters considered here, a reduction of about 100% in the peak shear stress and about 110% in the peak peel stress is observed both from FEA and analytical model. A significant decrease in the shear and peel stresses is attributed to huge variation in the bondline stiffness, from $E_m = 3.92$ GPa to $E_0 = 0.28$ GPa. From Figs. 3, it should be noted that for the cases of both graded and non-tailored bondlines with titanium adherends, for the parameters chosen here, the bondlength $l = 50$ mm can be regarded as the critical shear-transfer-length. The following sub-sections discuss the validation of the proposed deterministic models.

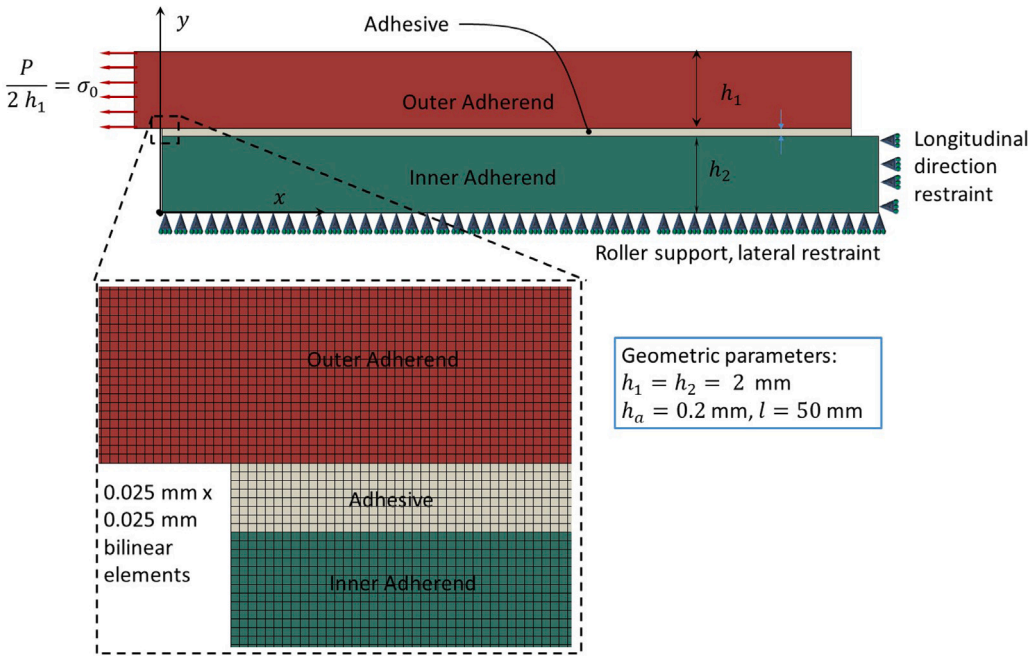

Fig. 2. Finite Element Model: Schematic representation of the FE model with appropriate loading and boundary conditions.

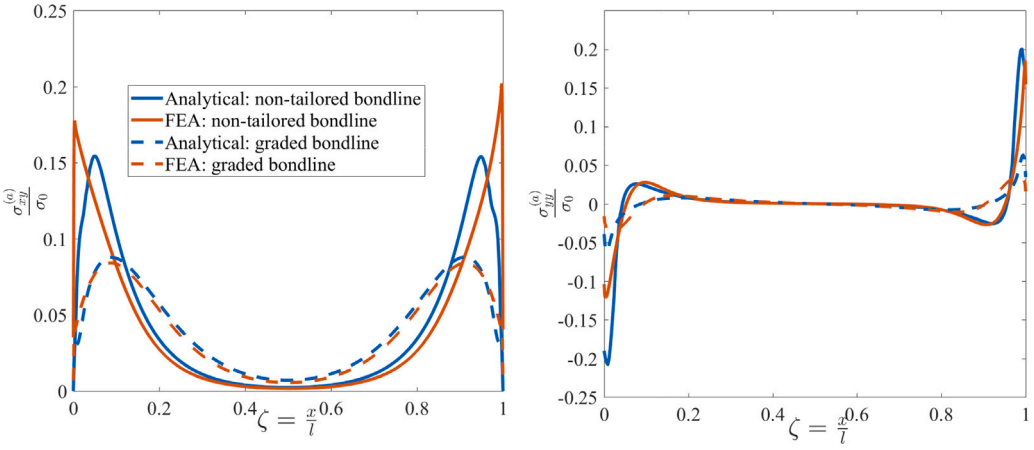

Fig. 3. Analytical vs FEA: (a) normalized shear stress distribution and (b) normalized peel stress distribution along the overlap length at the mid-surface of the adhesive for DLJs comprising titanium adherends with non-tailored (epoxy adhesive) and graded bondlines.

Table 2
Material properties of adherends and adhesive (Da Silva and Adams, 2007): The geometric properties for baseline case are $l = 50$ mm, $h_1 = h_2 = 2$ mm, and $h_a = 0.2$ mm. The DLJ comprises titanium adherends and epoxy adhesive. Note that $i = 1, 2$ refers to top and middle adherend, respectively and NA (not applicable) refers to a dependent constant. The graded epoxy adhesive with assumed modulus profiles is considered for exploration.

	Modulus of elasticity (GPa)	Shear modulus (GPa)	Poisson's ratio	Coefficient of thermal expansion (10^{-6} °C^{-1})
Titanium adherend	$E^{(i)} = 106.3$	NA	$\nu^{(i)} = 0.34$	$\alpha^{(i)} = 8.5$
BMI 2 × 2 twill weave Composite adherend	$E_x^{(i)} = E_z^{(i)} = 59.54$, $E_y^{(i)} = 10$	$G_{xy}^{(i)} = G_{yz}^{(i)} = G_{xz}^{(i)} = 7$	$\nu_{xy}^{(i)} = 0.3$ $\nu_{yz}^{(i)} = 0.05$ $\nu_{xz}^{(i)} = 0.05$	$\alpha_x^{(i)} = \alpha_z^{(i)} = 4.2$ $\alpha_y^{(i)} = 34.4$
Epoxy adhesive Non-tailored	$E^{(a)} = 3.45$	NA	$\nu^{(a)} = 0.36$	$\alpha^{(a)} = 58$
Epoxy adhesive Graded	$E_c = 3.45$, $E_0 = 0.28$ See Eq. (36)	NA	$\nu^{(a)} = 0.36$ (assumed)	$\alpha^{(a)} = 58$ (assumed)

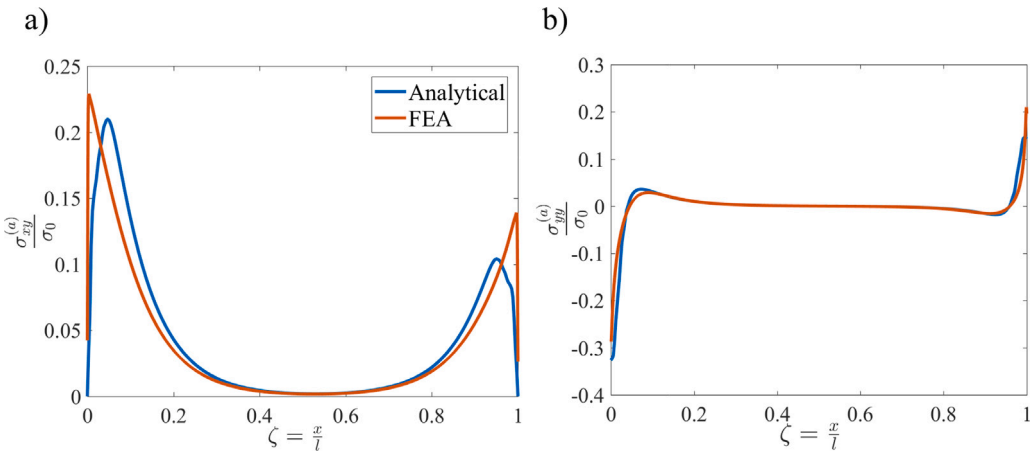

Fig. 4. Analytical vs FEA: Shear and peel stress distribution at the midsurface of a non-tailored epoxy adhesive for a composite-to-titanium DLJ.

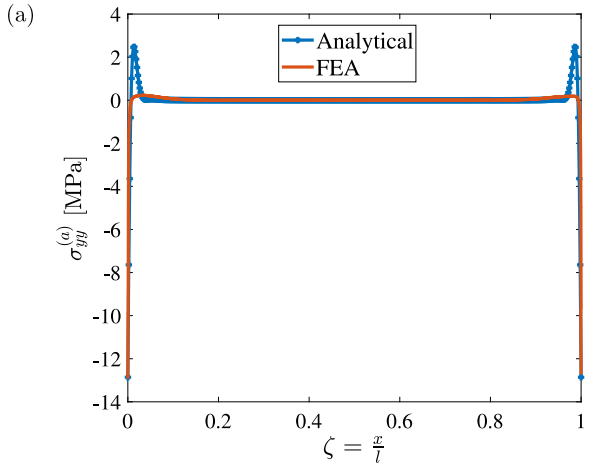

Fig. 5. Analytical vs FEA: Peel stress distribution at the midsurface of a non-tailored epoxy adhesive with titanium adherends subjected to pure thermal loading. The temperature is uniformly changed from 0° to −113 °C.

4.3. Metal-to-composite joints subjected to mechanical loading

The predictions of the proposed deterministic model are further validated against FE results, for the case of titanium adherend in the middle bonded to composite top and bottom adherends (BMI 2 × 2 twill weave, see Table 2 for properties) using an Epoxy adhesive subjected to an axial tensile load. Fig. 4a and 4b presents the shear and peel stress distributions, respectively, predicted by the proposed model. It can be noted that the predicted distribution and peaks of the shear and the peel stresses are in good agreement with the FE solution.

4.4. Metal-to-metal joints subjected to thermal loading

The deterministic DLJ model is further validated for the case of joint subjected to pure thermal loading. For this example, the DLJ assembly comprised Titanium adherends and an Epoxy adhesive. The temperature of the system was uniformly changed from 0 to −113 °C. Fig . 5 shows the peel stresses at the mid-surface of the adhesive along the overlap length, evaluated both from the proposed model and the FEA. The proposed model accurately captures the stress peaks as evidenced by the FE results. Higher accuracy of the proposed model could be attributed to negligible bending deformations. This observation is in-line with the simplifying assumption employed in formulating the governing equations.

5. Results and discussion

The solution for stresses in the DLJ based on the stochastic model is discussed in this section, and the effect of uncertainties in the modulus profiles of homogeneous and tailored adhesives on the stresses is analyzed. For the simulations, we used non-intrusive stochastic collocation method with sparse grid level four. Furthermore, the shear and peel stresses were expanded using a polynomial chaos expansion with dimension eight and order three.

5.1. Stochastic bondline with homogeneous mean (SBHM), $E^{(a)}(\omega)$

As discussed before, in order to predict the variability in the adhesive shear and peel stresses for conventional DLJs with homogeneous adhesive, analyses were carried out by treating the adhesive as a stochastic bondline with a homogenous/constant mean (SBHM) elastic modulus, $E^{(a)}$ with a coefficient of variation (CoV) δ and a correlation length $l/4$ (similar stochastic variables were adopted by Tipireddy and Kumar, 2017). The modulus profile of SBHM, its respective deviations and a few realizations, for the parameters considered here are presented in Fig. 6a and 6b. The CoV of the Young's modulus of Epoxy adhesives is in the order of 0.1 to 0.15 (Sanei and Fertig, 2016; Yurdakul et al., 2020). Higher values of CoV could be expected when the adhesives are exposed to thermal cycles, higher temperatures, and hydrothermal cycles (Qin et al., 2022). Therefore, we made a judicious choice to study the CoV of the adhesive modulus up to 0.2. The geometric and material properties adopted for this example are presented in Table 2. The effect of varying δ on the adhesive shear stress distribution is plotted in Fig. 7a for values of δ ranging from 0.05 to 0.2. Here, the solid line represents the mean of the normalized shear stresses as a function of the overlap length. The stochastic variations in the shear stress distribution is represented as lower and upper bounds using dashed lines. Fig. 7b and 7c shows the Probability Density Function (PDF) and Cumulative Distribution Function (CDF), respectively, of the normalized peak shear stress in the adhesive as a function of CoV, δ of the elastic modulus of the adhesive. Note that the PDFs are used here to compute the standard deviations and CoVs of the peak adhesive stresses. It can be clearly seen from Fig. 7a and 7b, that with the changes in CoV, δ of the elastic modulus of the adhesive, the mean of the shear stress distribution remains unchanged, while the standard deviation of the shear stresses increases with the increase in δ which is expected. The standard deviation of the normalized peak shear stress increases from 0.0023 to 0.0102 as δ increases from 0.05 to 0.2. Concomitantly, the CoV of the peak shear stress increases from 0.0154 to 0.0607 as the δ changes from 0.05 to 0.2. The distribution of peel stress and its variability as a function of CoV, δ of the elastic modulus of adhesive along with PDFs and CDFs of peek peel stresses presented in Fig. 8, shows a similar behavior to that

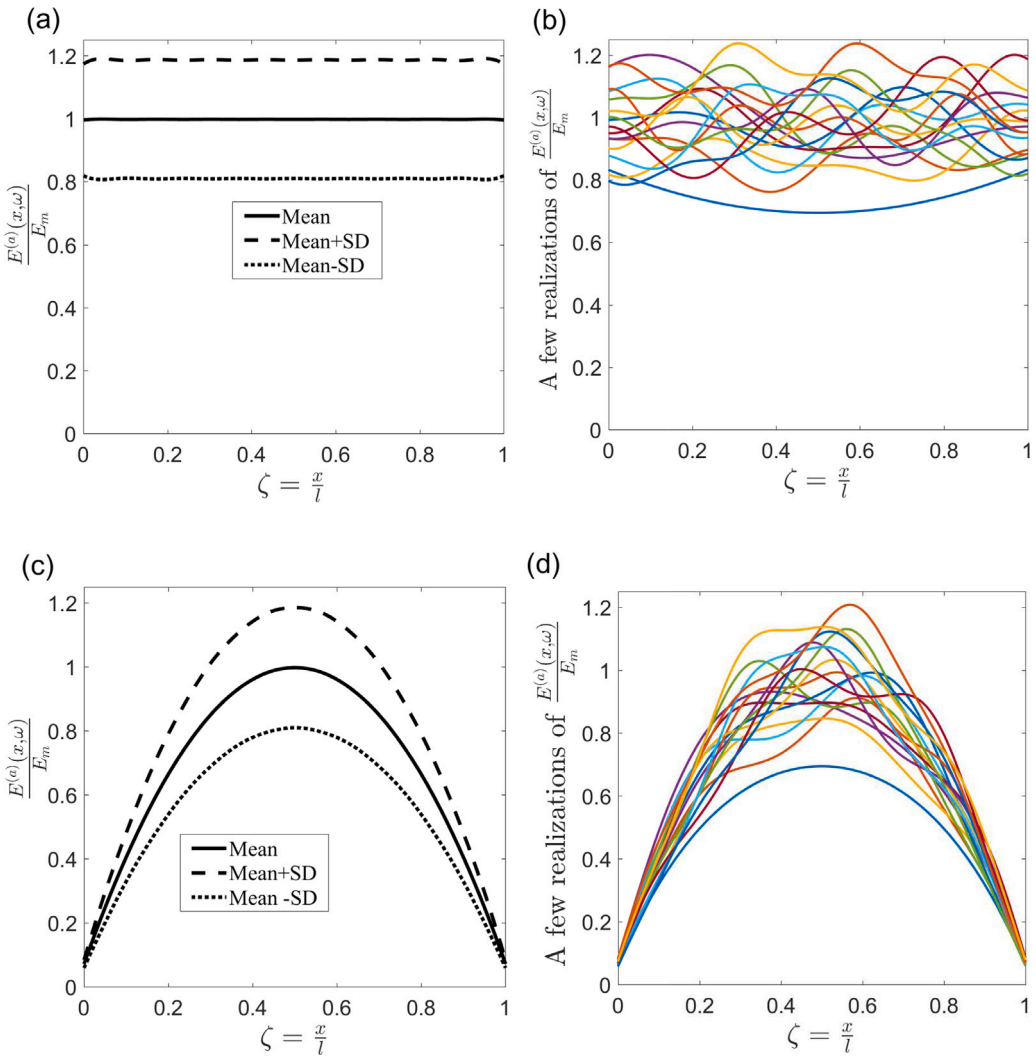

Fig. 6. (a) Spatial distribution of mean values of elastic modulus of homogeneous adhesive and its stochastic variations, (b) A few realizations of elastic modulus of homogeneous adhesive, (c) Spatial distribution of mean values of elastic modulus of tailored adhesive and its stochastic variations, and (d) A few realizations of elastic modulus of tailored adhesive; for $\delta = 0.2$, correlation length $= \frac{l}{4}$.

of the variability in shear stresses. In Fig. 8a, the solid line represents the mean of the normalized peel stresses as a function of the overlap length while the stochastic variation of the peel stresses are represented by dashed lines. The standard deviation of the normalized peak peel stress increases from 0.0028 to 0.0093 as δ varies from 0.05 to 0.2. Consequently, the CoV of the peak peel stress increases from 0.0133 to 0.0509 as δ changes from 0.05 to 0.2. Note that, for a DLJ with the parameters considered here, the relative standard deviations and the CoVs of peak shear and peel stresses, arising due to a CoV, δ in the elastic modulus of the adhesive, treated as SBHM, are similar in magnitude.

In the following discussion, variability in the shear and peel stresses as a function of geometric and material properties of a DLJ is discussed. Keeping all the other parameters constant, adhesive stresses are analyzed for a DLJ with SBHM having mean $E^{(a)} = 3450$ MPa and CoV, $\delta = 0.2$. As discussed in the preceding section, the critical shear-transfer-length is 50 mm for the parameters chosen here and therefore DLJs with bondlengths $l = \{50, 75, 100\}$ mm are analyzed. The PDFs of peak adhesive stresses along the mid-surface of the adhesive, near the free edges are evaluated as a function of l and are plotted in Figs. 9a and 9b. From Fig. 9a, a decrease followed by saturation in the mean value of the shear stress peaks is observed as the bondlength is increased from 50 to 100 mm. A reduction in standard deviation of the normalized peak shear stress from about 0.009 to 0.006 is noted as the bondlength is increased from 50 to 100 mm. Concomitantly, a reduction in CoV of the normalized peak shear stress from about 0.0607 to 0.0395 is noted as the bondlength is increased from 50 to 100 mm. It is further observed from Fig. 9b that the mean value of the peak peel stress decreases and saturates as the bondlength is increased from 50 to 100 mm. However, the standard deviation of the peak peel stress remains almost the same (0.0102 to 0.0123) as the bondlength is increased from 50 to 100 mm. Previous studies (Khan et al., 2018b; Kumar and Khan, 2016a) have reported that the peak stress decreases and saturates as the bondlength increases. Note that the standard deviation of the peak shear stress decreases to a constant value as a bondlength l increases above the critical or full stress-transfer-length while the standard deviation of the peak peel stress remains the same as the bondlength is increased above the critical shear-transfer-length (l_{cr}). The CoV of the peak peel stress also remains similar, ranging between 0.051 and 0.062 as the bondlength is increased from 50 to 100 mm.

An important parameter in the design of an adhesively bonded joint is its adhesive thickness as discrepancy in the performance of joints from experimental and theoretical studies, with respect to adhesive thickness is often reported (da Silva et al., 2006). da Silva et al. (2006) demonstrated through experimental evaluation that bonded assemblies with thin adhesives are tougher while the theoretical or numerical

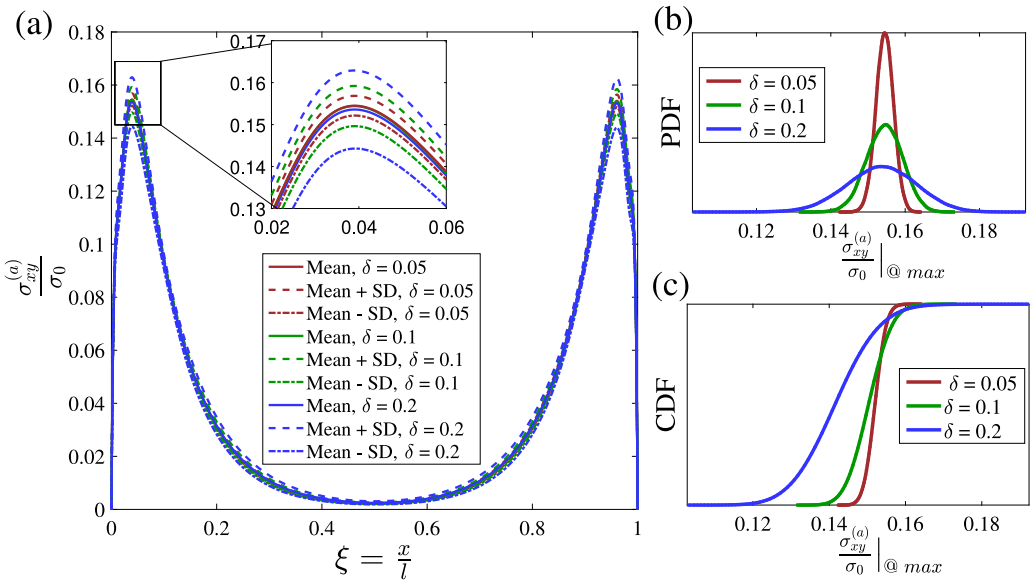

Fig. 7. DLJs with SBHM: (a) Spatial distribution of mean values of shear stresses and their stochastic variations at the mid-surface of the adhesive with titanium adherends subjected to mechanical loading for different choices of CoV δ of the elastic modulus of the adhesive. (b) PDFs, and (c) CDFs; of the normalized peak shear stresses in the adhesive.

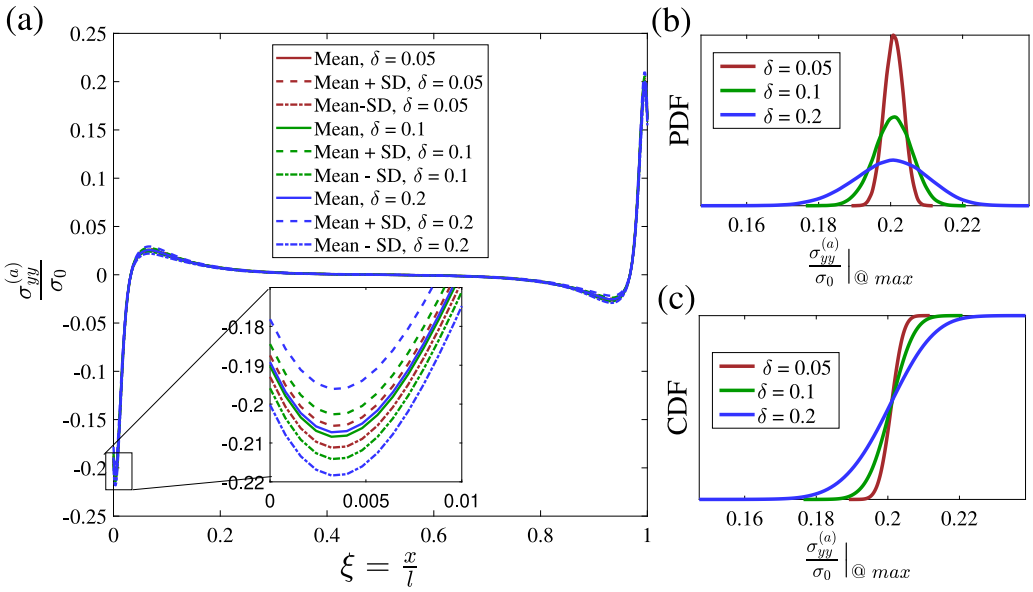

Fig. 8. DLJs with SBHM: (a) Spatial distribution of mean values of peel stresses and their stochastic variations at the mid-surface of the adhesive with titanium adherends subjected to mechanical loading for different choices of CoV δ of the elastic modulus of the adhesive. (b) PDFs, and (c) CDFs; of the normalized peak peel stresses in the adhesive.

techniques (see for instance Kumar, 2009) predicts that the joints with relatively thick adhesives are stronger. This discrepancy is ascribed to the size effect of thin adhesives which is not usually captured by models. The effect of varying the adhesive thickness on the deviation in the adhesive stresses of a DLJ with SBHM having a CoV, $\delta = 0.2$ is examined by parameterically varying adhesive thicknesses h_a in the range $\{0.1, 0.2, 0.3, 0.5\}$ mm while maintaining all the other parameters from Table 2, the same. Fig. 10a shows the PDFs of shear stress peak for different choices of adhesive thickness h_a for non-tailored adhesive with titanium adherends. It can be observed that the mean of the peak shear stress is reduced with the increase in adhesive thickness h_a. The standard deviation of the normalized peak shear stresses could be considered as a constant value (by observing the PDFs) as they are ranging within 0.0087 and 0.0094 with the increase in the adhesive thickness from 0.1 to 0.5 mm. However, the CoV of the peak shear stress increases from 0.054 to 0.0776 as the adhesive thickness increases from 0.1 to 0.5 mm. From Fig. 10b, the mean of peak peel stress decreases with the increase in adhesive thickness as reported elsewhere (Khan et al., 2018b; Kumar and Khan, 2016a). The standard deviations computed from PDFs in Fig. 10b are $\{0.0087, 0.0103, 0.0105, 0.0102\}$ for $h_a = \{0.1, 0.2, 0.3, 0.5\}$ mm, respectively, indicating that it increases with the adhesive thickness up to certain value and then saturates with a further increase in thickness. The CoV of the peak peel stress increases from about 0.0348 to 0.0731 as the adhesive thickness is increased from 0.1 to 0.5 mm.

The adhesive stresses in DLJ are further analyzed by treating the adhesive modulus as a stochastic field $E^{(a)}(\omega)$ with constant means = $\{1000, 2000, 3450\}$ MPa and CoV $\delta = 0.2$ while maintaining all the other parameters (given in Table 2), the same. As the bondline stiffness is increased or decreased, the critical shear-transfer-length will decrease or increase, accordingly (Khan et al., 2018b). Hence, it is important to look at the complete distribution of the shear and peel stresses in

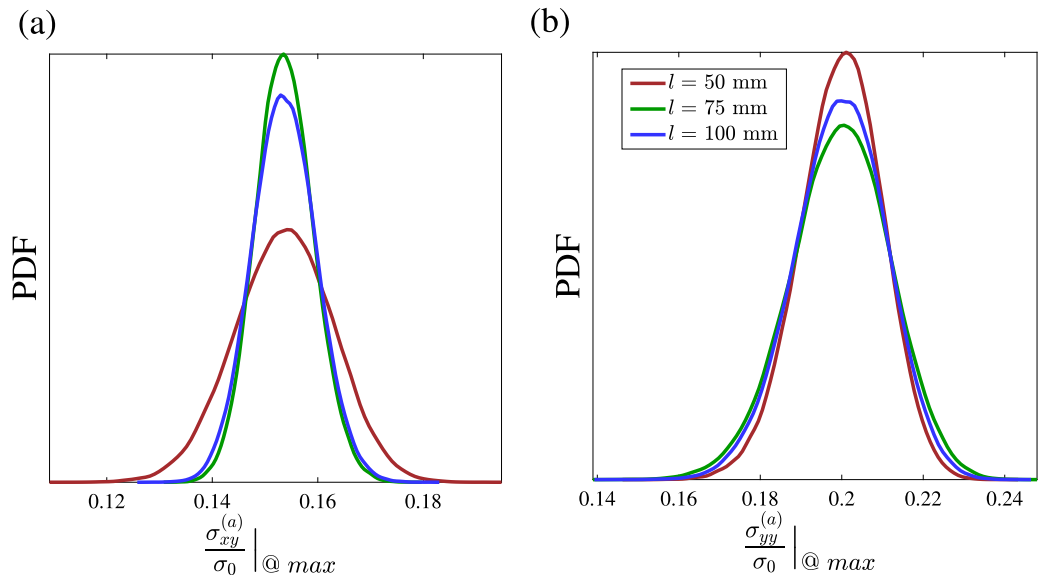

Fig. 9. DLJs with SBHM: (a) PDFs of normalized peak shear stress and (b) PDFs of normalized peak peel stress at the mid-surface of the adhesive with titanium adherends subjected to mechanical loading for different choices of overlap length l.

order to identify the critical shear-transfer-length. The shear stresses along the mid-surface of the adhesive, for different choices of adhesive modulus, are plotted in Fig. 11a. The following observations could be made

- The mean of peak shear stresses and their gradients increase with an increase in adhesive stiffness which is in agreement with the observations made by the previous studies on bonded joints (see for instance Kumar and Khan, 2016a).
- For the mean adhesive moduli $E^{(a)} = \{1000, 2000\}$ MPa, the left-end of the joint ($\zeta = 0$), where the top adherend continues, shows a smaller standard deviation of the normalized peak shear stress relative to the right-end of the joint.
- For an increased mean of the adhesive modulus $E^{(a)} = 3450$ MPa, the standard deviations of the normalized peak shear stress are the same at both the edges of the joint.

The PDFs and CDFs of the normalized peak shear stress at the right-edge, of the DLJ, presented in Fig. 11b and 11c, shows that the standard deviation of the peak shear stress decreases with an increase in adhesive stiffness for the parameters chosen here. The standard deviation of the normalized peak shear stress decreases from 0.0115 to 0.0093 as the mean adhesive modulus is increased from 1000 to 3450 MPa. As a result, the CoV of the peak shear stress decreases from about 0.1127 to 0.0607 as the adhesive modulus is increased from 1000 to 3450 MPa. Fig. 12a, shows the distribution of adhesive peel stresses for different choices of mean value of the adhesive modulus $E^{(a)} = \{1000, 2000, 3450\}$ MPa. It shows similar behavior as that of the shear stress distribution. Fig. 12b and 12c provides the PDFs and CDFs of the normalized peak peel stresses for different choices of adhesive modulus. It can be noted from PDFs in Fig. 12b that the standard deviation of the normalized peak peel stress reduces from 0.0163 to 0.0102 as the mean adhesive modulus is increased from 1000 to 3500 MPa. Concomitantly, CoV of the peak peel stress decreases from 0.1179 to 0.0509 as the mean adhesive modulus is increased from 1000 MPa to 3450 MPa. Therefore, it can be concluded that the variation in adhesive peak stresses reduces as the bondline stiffness increases.

5.2. Stochastic bondline with tailored mean, $E^{(a)}(x, \omega)$

In the validation section, we have demonstrated the effectiveness of a graded bondline in reducing the stress concentrations near the free edges of a DLJ as reported exhaustively in the extant works for various bonded assemblies (Kumar and Adams, 2017; Stein et al., 2017). As discussed before, realizing desired stiffness of a graded bondline exactly is challenging as the gradation is primarily controlled through curing. In practice, achieving a functionally graded profile is envisaged to have relatively higher uncertainty than a homogeneous bondline due to considerations such as flow of adhesives, the curing kinetics etc. Henceforth, the adhesive is considered as a spatially varying stochastic field with a parabolic distribution of mean stiffness given by Eq. (36) with a CoV, δ and a correlation length of $l/4$ (similar stochastic variables were adopted by Tipireddy and Kumar, 2017). This bondline is henceforth referred to as stochastic bondline with tailored mean (SBTM). The modulus profile of SBTM, its respective deviations and a few realizations, for the parameters considered here are plotted in Fig. 6c and 6d. The PDF of the peak shear and peel stresses as a function of CoV, δ of the elastic modulus of the adhesive for the DLJ with SBTM plotted in Fig. 13a and 13b, showcases similar trend to that of non-tailored bondline. Fig. 13a, shows that the standard deviation of the normalized peak shear stress increases from 0.0016 to 0.0065 as δ varies from 0.05 to 0.2. Consequently, the CoV of the peak shear stress increases from 0.0186 to 0.0745 as δ changes from 0.05 to 0.2. Similarly, from Fig. 13b, the standard deviation of the normalized peak peel stress increases from 0.0018 to 0.0072 as the δ increases from 0.05 to 0.2. The CoV of the peak peel stress increases from 0.0288 to 0.1148 as the δ changes from 0.05 to 0.2.

To study the effect of bondlength on the peak adhesive stresses and their respective variations for a DLJ with SBTM, maintaining all other parameters constant and $\delta = 0.2$, analyses were carried out by varying overlap lengths $l = \{50, 75, 100\}$ mm. Fig. 14a shows PDFs of the peak shear stress as a function of l. It can be clearly seen that the mean and standard deviation of the peak shear stress decrease with the increase in overlap length l. In contrast to the SBHM, the standard deviation in peak shear stress does not saturate with the increase in bondlength up to 100 mm. The standard deviation of the normalized peak shear stress decreases from 0.0065 to 0.0056 as the overlap length increases from 50 to 100 mm. The CoV of the peak shear stresses remains almost the same, ranging from 0.0745 to 0.077 as bondlength increases from 50 to 100 mm. Fig. 14b shows the PDF of the normalized peak peel stress for the joints with SBTM having a parabolic mean and a CoV $\delta = 0.2$, as a function of overlap length $l = \{50, 75, 100\}$ mm. It can be observed that the standard deviation of the normalized peak peel

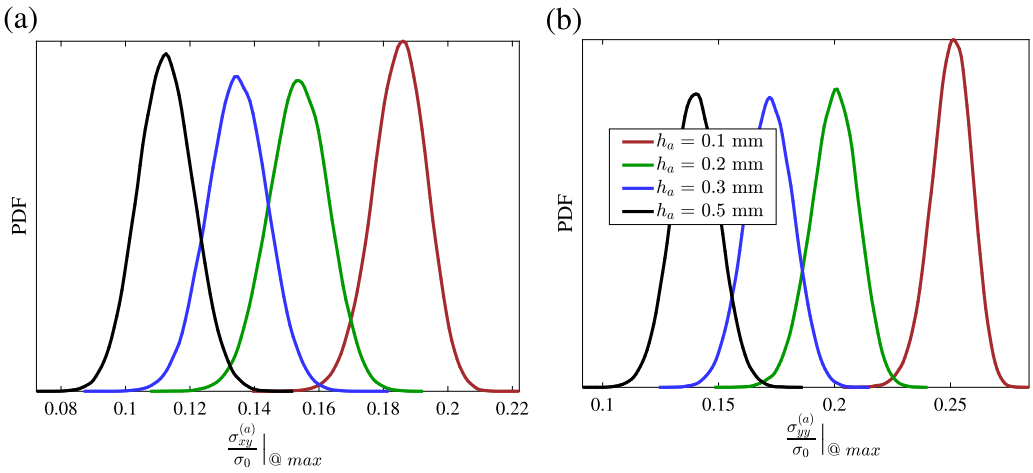

Fig. 10. DLJs with SBHM: (a) PDFs of normalized peak shear stress and (b) PDFs of normalized peak peel stress; at the mid-surface of the adhesives with titanium adherends subjected to mechanical loading for different choices of adhesive thickness h_a.

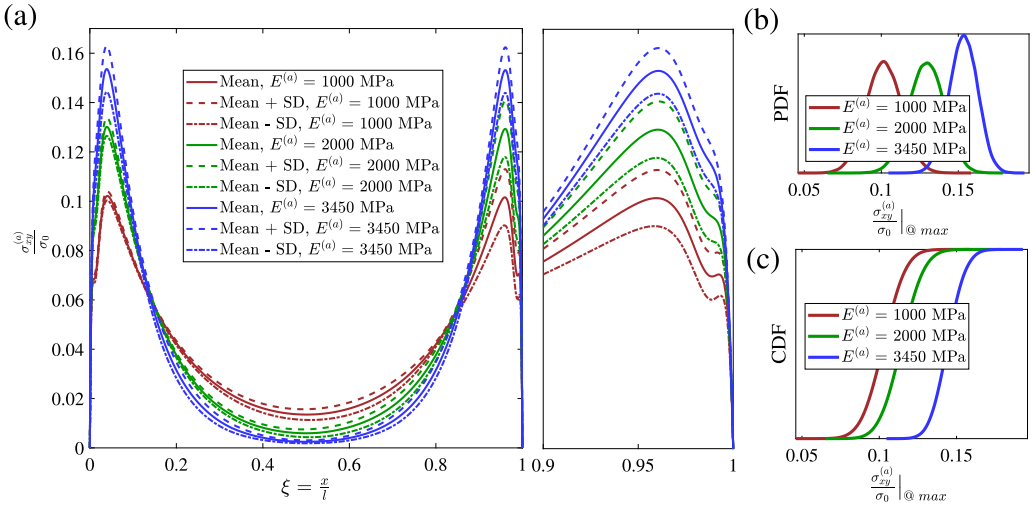

Fig. 11. DLJs with SBHM: (a) Spatial distribution of mean values of shear stresses and their stochastic variations at the mid-surface of the adhesives with titanium adherends subjected to mechanical loading for different choices of mean value of the adhesive modulus $E^{(a)}$. (b) PDFs and (c) CDFs; of the normalized peak shear stress in the adhesive.

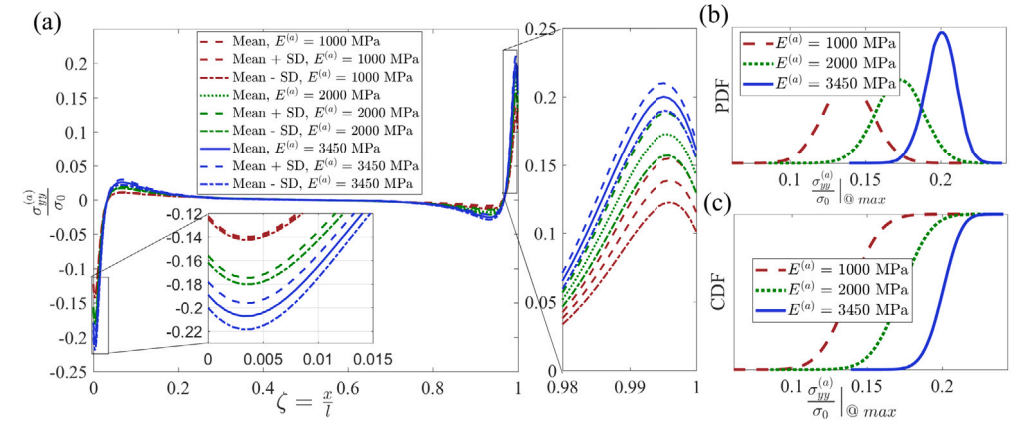

Fig. 12. DLJs with SBHM: (a) Spatial distribution of mean values of peel stresses and their stochastic variations at the mid-surface of the adhesive with titanium adherends subjected to mechanical loading for different choices of mean value of the adhesive modulus $E^{(a)}$. (b) PDFs and (c) CDFs; of normalized peak peel stress in the adhesive.

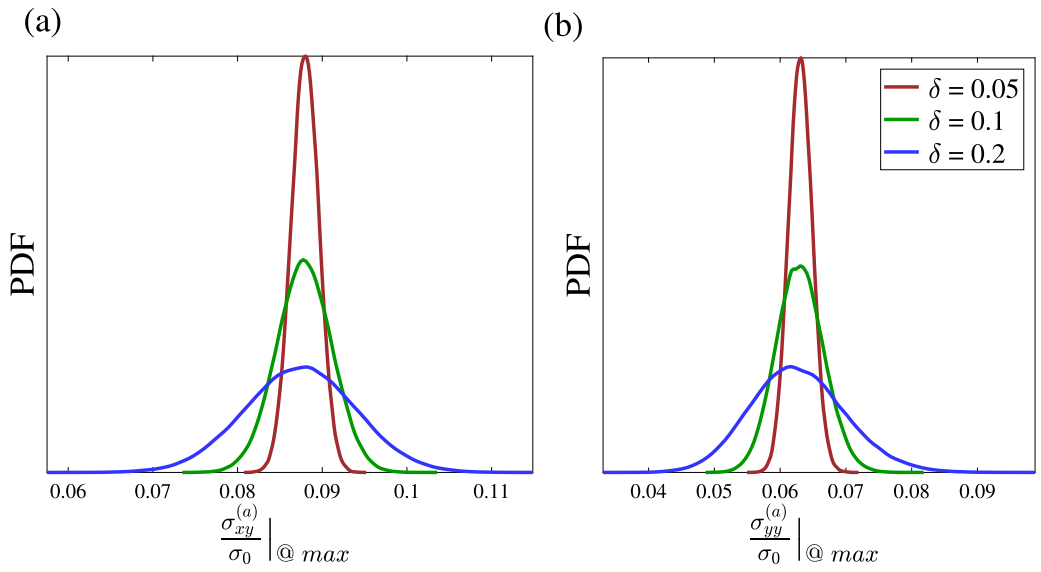

Fig. 13. DLJs with SBTM: (a) PDFs of the normalized peak shear stress and (b) PDFs of the normalized peak peel stress at the mid-surface of the adhesive with titanium adherends subjected to mechanical loading for different choices of coefficient of variation δ in the elastic modulus of the adhesive.

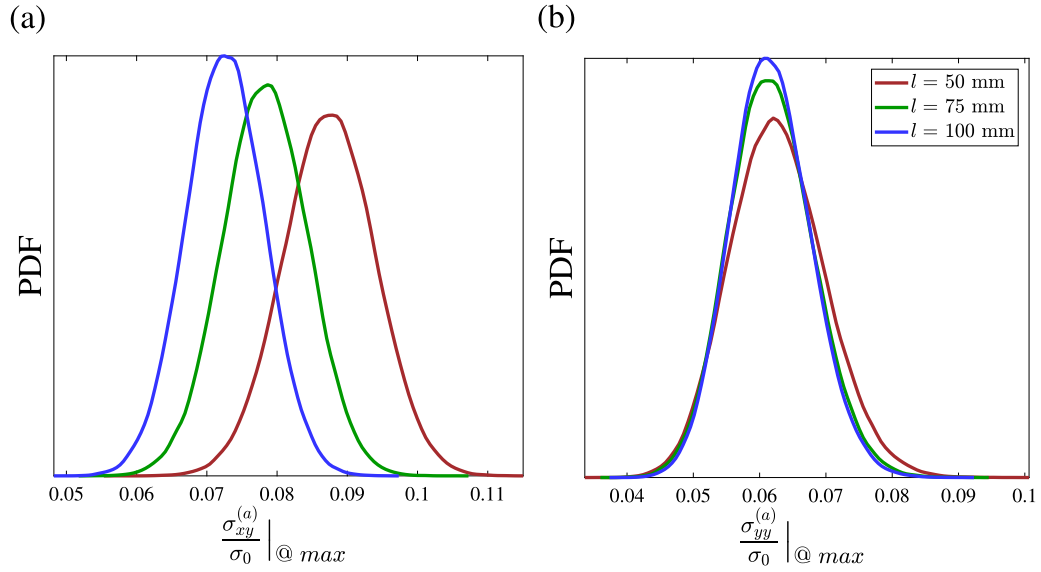

Fig. 14. DLJs with SBTM: (a) PDFs of the normalized peak shear stress and (b) PDFs of normalized peak peel stress at the mid-surface of the adhesive with titanium adherends subjected to mechanical loading for different choices of an overlap length l.

stress decreases and nearly saturates with an increase in overlap length l while the mean values of the normalized peak peel stresses remain the same. The standard deviation of the normalized peak peel stress decreases from 0.0071 to 0.0060 as the bondlength increases from 50 to 100 mm. It can also be noted from Fig. 14b and 14c that the standard deviation of the normalized peak peel stress saturates for bondlengths larger than shear-transfer-length for the DLJs with SBTM. The CoV of the peak peel stress marginally decreases from 0.1138 to 0.0976 as the bondlength is increased from 50 to 100 mm.

The effect of bondline thickness on the adhesive stresses for the joint with SBTM was evaluated by varying the adhesive thickness in the range $h_a = \{0.1, 0.2, 0.3, 0.5\}$ mm, while all the other parameters were kept the same. For this case, the PDF of normalized peak shear stress in the adhesive presented in Fig. 15a, shows that the mean value of peak shear stress decreases with increase in adhesive thickness. It can further be noted that the standard deviation of the normalized peak shear stress decreases with increase in adhesive thickness. The standard deviation computed from Fig. 15a of the normalized peak shear stress decreases from 0.0078 to 0.0056 as the bondline thickness is increased from 0.1 to 0.5 mm. However, the CoV of the peak shear stress increases marginally from 0.0714 to 0.0804 as the bondline thickness increases from 0.1 to 0.5 mm. Fig. 15b shows the PDF of the normalized peak peel stress as a function of adhesive thickness, for the DLJ with SBTM and it shows similar behavior as that of PDF of the normalized peak shear stress as a function of adhesive thickness. The mean value of the peak peel stress decreases as a function of bondline thickness h_a and the standard deviation of the normalized peak peel stress decreases from 0.0099 to 0.0049 as the bondline thickness is increased from 0.1 to 0.5 mm. However, the CoV of the normalized peak peel stress increases from 0.1030 to 0.1277 as the bondline thickness increases from 0.1 to 0.5 mm.

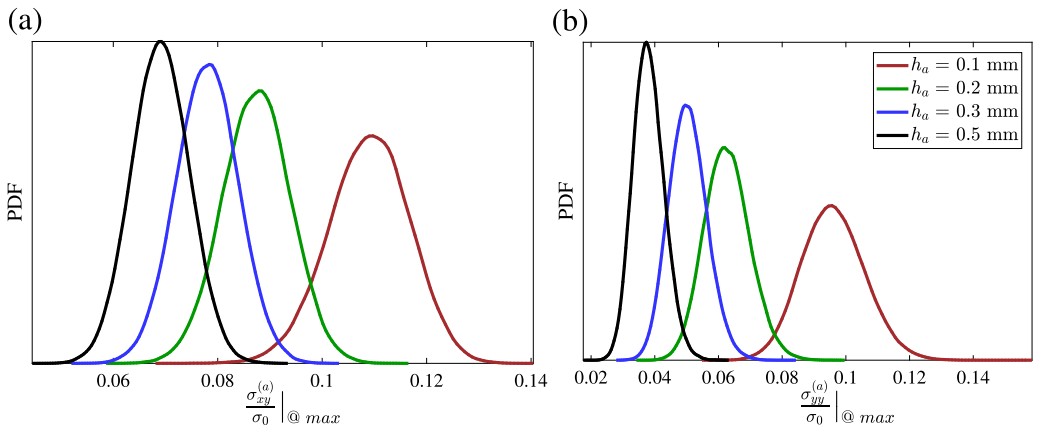

Fig. 15. DLJs with SBTM: (a) PDFs of normalized peak shear stress and (b) PDFs of normalized peak peel stress at the mid-surface of the adhesive with titanium adherends subjected to mechanical loading for different choices of adhesive thickness h_a.

6. Conclusions

A generic plane-stress/plane-strain model is proposed for predicting the stresses in adhesively bonded double-lap joints (DLJs) with a functionally graded bondline. The model is then reformulated in probabilistic mechanics framework where the modulus of adhesive is regarded as a spatially varying random field both with homogeneous and tailored mean. The validation of the proposed stress-based formulation in deterministic framework for the DLJ with homogeneous and functionally graded bondlines is carried out against the results obtained from an analogous Finite Element (FE) model for a range of joints consisting of metallic and composite adherends, under mechanical and thermal loadings. The predictions of the proposed model are in good agreement with the FE results. The uncertainty quantification was carried out for two cases viz 1. stochastic bondline with homogenous mean (SBHM) and 2. stochastic bondline with tailored/graded mean (SBTM) representing uncertainties in conventional and functionally graded double-lap bonded assemblies, respectively. The analyses were carried out to determine the mean of adhesive shear and peel stress distribution and the PDFs of respective peak stresses as a function of coefficient of variation (CoV) of the elastic modulus of the adhesive, bondlength, adhesive thickness and adhesive stiffness, in the presence of a stochastic bondline. From these results, the following observations were made:

- The CoVs of the peak shear stress are about 0.0607 and 0.0745, respectively, for joints with SBHM and SBTM, due to a CoV of 0.2 in the elastic modulus of the adhesive. Therefore, a similar variation in shear stress in the graded and non-tailored bondlines is noted.
- The CoVs of the peak peel stress are about 0.0509 and 0.1148, respectively, for joints with SBHM and SBTM, respectively, due to a coefficient of variation of 0.2 of the elastic modulus of the adhesive. Therefore, higher variations in peel stresses are reported for DLJs with graded adhesives.
- The standard deviations and the CoVs of the normalized peak shear stress decrease with the increase in bondlength while the standard deviations and the CoVs of the normalized peak peel stress, remain almost the same for joints with SBHM.
- The CoVs of normalized peak shear and peel stresses are almost constant with respect to changes in bondlength above the critical shear transfer length for joints with SBTM.
- The standard deviation of the shear and peel stresses remains more or less constant with the change in thickness for the joints with SBHM/SBTM.
- The standard deviations and the CoVs of the adhesive peak stresses decrease significantly with the increase in adhesive stiffness.

CRediT authorship contribution statement

M.A. Khan: Software, Validation, Formal analysis, Investigation, Data curation, Writing – original draft, Writing – review & editing. **R. Tipireddy:** Software, Validation, Formal analysis, Investigation, Data curation, Writing – original draft, Writing – review & editing. **B. Dattaguru:** Validation, Visualization, Writing – original draft. **S. Kumar:** Conceptualization, Methodology, Formal analysis, Investigation, Resources, Writing – original draft, Writing – review & editing, Supervision.

Declaration of competing interest

The authors declare that they have no known competing financial interests or personal relationships that could have appeared to influence the work reported in this paper.

Data availability

No data was used for the research described in the article.

Acknowledgments

S. K. would like to thank the University of Glasgow, United Kingdom for the start-up grant (Award No: 144690-1).

Appendix. Coefficients of the governing ODE

$$A_{\alpha\beta} = \begin{bmatrix} 2\phi_5 & \phi_{10} \\ \phi_{10} & 2\phi_6 \end{bmatrix}; \quad B_{\alpha\beta} = \begin{bmatrix} 4\phi_5' & 2\phi_{10}' \\ 2\phi_{10}' & 4\phi_6' \end{bmatrix}$$

$$C_{\alpha\beta} = \begin{bmatrix} 2\phi_8 - 2\phi_3 + 2\phi_5'' & -\phi_7 + \phi_{10}'' \\ -\phi_7 + \phi_{10}'' & \phi_9 - 2\phi_4 + 2\phi_6'' \end{bmatrix}$$

$$D_{\alpha\beta} = \begin{bmatrix} -2\phi_3' + 2\phi_8' & -\phi_7' \\ -\phi_7' & -2\phi_4' + 2\phi_9' \end{bmatrix}; \quad F_{\alpha\beta} = \begin{bmatrix} 2\phi_1 + \phi_8'' & 0 \\ 0 & 2\phi_2 + \phi_9'' \end{bmatrix}$$

$$J_\alpha = \begin{pmatrix} \phi_{11} + \phi_{13}'' \\ \phi_{12} + \phi_{14}'' \end{pmatrix}$$

References

Adams, R.D., 2018. Nondestructive testing. In: da Silva, L.F.M., Öchsner, A., Adams, R.D. (Eds.), Handbook of Adhesion Technology. Springer International Publishing, Cham, pp. 1171–1194.

Adams, R.D., Peppiatt, N.A., 1974. Stress analysis of adhesive-bonded lap joints. J. Strain Anal. Eng. Des. 9 (3), 185–196.

Babuška, I., Chatzipantelidis, P., 2002. On solving elliptic stochastic partial differential equations. Comput. Methods Appl. Mech. Engrg. 191 (37–38), 4093–4122.

Babuška, I., Nobile, F., Tempone, R., 2007. A stochastic collocation method for elliptic partial differential equations with random input data. SIAM J. Numer. Anal. 45 (3), 1005–1034.

Bhat, M.R., et al., 2015. Probabilistic stress variation studies on composite single lap joint using Monte Carlo simulation. Compos. Struct. 121, 351–361.

Carbas, R.J.C., Da Silva, L.F.M., Critchlow, G.W., 2014. Adhesively bonded functionally graded joints by induction heating. Int. J. Adhes. Adhes. 48, 110–118.

Carbas, R.J.C., da Silva, L.F.M., Andrés, L., 2017. Functionally graded adhesive joints by graded mixing of nanoparticles. Int. J. Adhes. Adhes..

Da Silva, L.F.M., Adams, R.D., 2007. Joint strength predictions for adhesive joints to be used over a wide temperature range. Int. J. Adhes. Adhes. 27 (5), 362–379.

Da Silva, L.F.M., Campilho, R.D., 2012. Advances in Numerical Modelling of Adhesive Joints. Springer.

Ghanem, R.G., Spanos, P.D., 1991. Stochastic finite element method: Response statistics. In: Stochastic Finite Elements: A Spectral Approach. Springer, pp. 101–119.

Goland, M., Reissner, E., 1944. The stresses in cemented joints. J. Appl. Mech. 11 (1), A17–A27.

Hart-Smith, L.J., 1973. Adhesive-Bonded Single-Lap Joints. Langley Research Center Hampton, VA.

Katnam, K.B., Stevenson, J.P.J., Stanley, W.F., Buggy, M., Young, T.M., 2011. Tensile strength of two-part epoxy paste adhesives: Influence of mixing technique and micro-void formation. Int. J. Adhes. Adhes. 31 (7), 666–673. http://dx.doi.org/10.1016/j.ijadhadh.2011.06.005, URL https://www.sciencedirect.com/science/article/pii/S0143749611000753.

Khan, M.A., Kumar, S., 2016. Interfacial stresses in single-side composite patch-repairs with material tailored bondline. Mech. Adv. Mater. Struct..

Khan, M.A., Kumar, S., 2018. Performance enhancement of tubular multilayers via compliance-tailoring: 3D printing, testing and modeling. Int. J. Mech. Sci. 140, 93–108. http://dx.doi.org/10.1016/j.ijmecsci.2018.02.038, URL http://www.sciencedirect.com/science/article/pii/S0020740317336056.

Khan, M.A., Kumar, S., Cantwell, W.J., 2018a. Additively manufactured cylindrical systems with stiffness-tailored interface: Modeling and experiments. Int. J. Solids Struct. 152–153, 71–84. http://dx.doi.org/10.1016/j.ijsolstr.2018.06.002, URL http://www.sciencedirect.com/science/article/pii/S0020768318302269.

Khan, M.A., Kumar, S., Reddy, J.N., 2018b. Material-tailored adhesively bonded multilayers: A theoretical analysis. Int. J. Mech. Sci. 148, 246–262. http://dx.doi.org/10.1016/j.ijmecsci.2018.08.017, URL http://www.sciencedirect.com/science/article/pii/S0020740318314395.

Khan, M.A., Wardle, B.L., Kumar, S., 2022. Elastic solutions for stresses in compliance-tailored adhesive anchors. Int. J. Adhes. Adhes. 118, 103227. http://dx.doi.org/10.1016/j.ijadhadh.2022.103227, URL https://www.sciencedirect.com/science/article/pii/S0143749622001440.

Kim, J., Kim, K.S., Kim, Y.H., 1989. Mechanical effects in peel adhesion test. J. Adhes. Sci. Technol. 3 (1), 175–187.

Kimiaeifar, A., Lund, E., Thomsen, O.T., Sørensen, J.D., 2013. Asymptotic sampling for reliability analysis of adhesive bonded stepped lap composite joints. Eng. Struct. 49, 655–663. http://dx.doi.org/10.1016/j.engstruct.2012.12.003, URL http://www.sciencedirect.com/science/article/pii/S0141029612006165.

Kimiaeifar, A., Toft, H., Lund, E., Thomsen, O.T., Sørensen, J.D., 2012a. Reliability analysis of adhesive bonded scarf joints. Eng. Struct. 35, 281–287.

Kimiaeifar, A., Toft, H., Lund, E., Thomsen, O.T., Sørensen, J.D., 2012b. Reliability analysis of adhesive bonded scarf joints. Eng. Struct. 35, 281–287. http://dx.doi.org/10.1016/j.engstruct.2011.11.013, URL http://www.sciencedirect.com/science/article/pii/S0141029611004512.

Kumar, S., 2009. Analysis of tubular adhesive joints with a functionally modulus graded bondline subjected to axial loads. Int. J. Adhes. Adhes. 29 (8), 785–795.

Kumar, S., Adams, R.D., 2017. Special issue on functionally graded adhesively bonded systems. Int. J. Adhes. Adhes. 76, 1–2. http://dx.doi.org/10.1016/j.ijadhadh.2017.05.002, Special Issue on Functionally Graded Materials. URL https://www.sciencedirect.com/science/article/pii/S014374961730088X.

Kumar, S., Khan, M.A., 2016a. An elastic solution for adhesive stresses in multi-material cylindrical joints. Int. J. Adhes. Adhes. 64, 142–152.

Kumar, S., Khan, M.A., 2016b. A shear-lag model for functionally graded adhesive anchors. Int. J. Adhes. Adhes. 68, 317–325.

Kumar, S., Mittal, K.L., 2013. Advances in Modeling and Design of Adhesively Bonded Systems. John Wiley & Sons.

Kumar, S., Pandey, P.C., 2010. Behaviour of bi-adhesive joints. J. Adhes. Sci. Technol. 24 (7), 1251–1281.

Kumar, S., Scanlan, J.P., 2013. On axisymmetric adhesive joints with graded interface stiffness. Int. J. Adhes. Adhes. 41, 57–72.

Kumar, S., Wardle, B.L., Arif, M.F., 2016. Strength and performance enhancement of bonded joints by spatial tailoring of adhesive compliance via 3D printing. ACS Appl. Mater. Interfaces.

Lévy, P., Loève, M., 1965. Processus Stochastiques et Mouvement Brownien. Gauthier-Villars Paris.

Luo, Y., Li, A., Kang, Z., 2011. Reliability-based design optimization of adhesive bonded steel–concrete composite beams with probabilistic and non-probabilistic uncertainties. Eng. Struct. 33 (7), 2110–2119.

Mathias, J.-D., Lemaire, M., 2013. Reliability analysis of bonded joints with variations in adhesive thickness. J. Adhes. Sci. Technol. 27 (10), 1069–1079.

Mortensen, F., Thomsen, O.T., 2002. Analysis of adhesive bonded joints: A unified approach. Compos. Sci. Technol. 62 (7), 1011–1031.

Olajide, S.O., Kandare, E., Khatibi, A.A., 2017. Fatigue life uncertainty of adhesively bonded composite scarf joints – an airworthiness perspective. J. Adhes. 93 (7), 515–530. http://dx.doi.org/10.1080/00218464.2015.1112796.

Omairey, S., Jayasree, N., Kazilas, M., 2021. Defects and uncertainties of adhesively bonded composite joints. SN Appl. Sci. 3 (9), 1–14.

Özer, H., Öz, Ö., 2017. The use of the exponential Drucker–Prager material model for defining the failure loads of the mono and bi-adhesive joints. Int. J. Adhes. Adhes..

Qin, G., Li, G., Mi, P., Zhu, Y., Li, M., Na, J., 2022. A systematic study on the failure behaviors of aluminum alloy/composite bonded joints exposed to various typical aging environments for automobiles. J. Adhes. 1–28. http://dx.doi.org/10.1080/00218464.2022.2141114.

Sanei, S.H.R., Fertig, R.S., 2016. Length-scale dependence of variability in epoxy modulus extracted from composite prepreg. Polym. Test. 50, 297–300. http://dx.doi.org/10.1016/j.polymertesting.2015.12.015, URL https://www.sciencedirect.com/science/article/pii/S0142941815301318.

da Silva, L.F.M., Lopes, M.J.C.Q., 2009. Joint strength optimization by the mixed-adhesive technique. Int. J. Adhes. Adhes. 29 (5), 509–514.

da Silva, L.F.M., Rodrigues, T.N.S.S., Figueiredo, M.A.V., de Moura, M.F.S.F., Chousal, J.A.G., 2006. Effect of adhesive type and thickness on the lap shear strength. J. Adhes. 82 (11), 1091–1115. http://dx.doi.org/10.1080/00218460600948511.

Stapleton, S.E., Waas, A.M., Arnold, S.M., 2012. Functionally graded adhesives for composite joints. Int. J. Adhes. Adhes. 35, 36–49.

Stein, N., Felger, J., Becker, W., 2017. Analytical models for functionally graded adhesive single lap joints: A comparative study. Int. J. Adhes. Adhes. 76, 70–82.

Stein, N., Weißgraeber, P., Becker, W., 2016. Stress solution for functionally graded adhesive joints. Int. J. Solids Struct. 97, 300–311.

Stroud, W., Krishnamurthy, T., Smith, S., 2002. Probabilistic and possibilistic analyses of the strength of a bonded joint. In: 19th AIAA Applied Aerodynamics Conference. p. 1238.

Tipireddy, R., Ghanem, R., 2014. Basis adaptation in homogeneous chaos spaces. J. Comput. Phys. 259, 304–317.

Tipireddy, R., Kumar, S., 2017. Spatially-degraded adhesive anchors under material uncertainty. Int. J. Adhes. Adhes..

Ubaid, J., Wardle, B.L., Kumar, S., 2018. Strength and performance enhancement of multilayers by spatial tailoring of adherend compliance and morphology via multimaterial jetting additive manufacturing. Sci. Rep. 8 (1), 13592.

Uddin, M.A., Alam, M.O., Chan, Y.C., Chan, H.P., 2004. Adhesion strength and contact resistance of flip chip on flex packages—effect of curing degree of anisotropic conductive film. Microelectron. Reliab. 44 (3), 505–514.

Xiu, D., Karniadakis, G.E., 2002. The Wiener–Askey polynomial chaos for stochastic differential equations. SIAM J. Sci. Comput. 24 (2), 619–644.

Yu, Q.-Q., Gu, X.-L., Zhao, X.-L., ming Zhang, D., wei Huang, H., Jiang, C., 2019. Characterization of model uncertainty of adhesively bonded CFRP-to-steel joints. Compos. Struct. 215, 150–165. http://dx.doi.org/10.1016/j.compstruct.2019.02.045, URL http://www.sciencedirect.com/science/article/pii/S0263822318318968.

Yurdakul, Ö., Tunaboyu, O., Routil, L., Avşar, Ö., 2020. Parameter sensitivity of CFRP retrofitted substandard joints by stochastic computational mechanics. Compos. Struct. 238, 112003. http://dx.doi.org/10.1016/j.compstruct.2020.112003, URL https://www.sciencedirect.com/science/article/pii/S0263822318346166.

Zhang, D., Gu, X.-L., Yu, Q.-Q., Huang, H., Wan, B., Jiang, C., 2018. Fully probabilistic analysis of FRP-to-concrete bonded joints considering model uncertainty. Compos. Struct. 185, 786–806. http://dx.doi.org/10.1016/j.compstruct.2017.11.058, URL http://www.sciencedirect.com/science/article/pii/S0263822317325114.